photonics

MDPI

Communication

Infrared Optical Vortices Generation with Holographic Optical Elements Recorded in Bayfol HX200 Photopolymer

Álvaro Paredes-Amorín [1], Julia Marín-Sáez [2,*], María-Victoria Collados [1] and Jesús Atencia [1]

[1] Applied Physics Department, Engineering Research Institute of Aragon (I3A), Faculty of Science, University of Zaragoza, Pedro Cerbuna 12, 50009 Zaragoza, Spain; vcollado@unizar.es (M.-V.C.); atencia@unizar.es (J.A.)
[2] Applied Physics Department, Escuela Politécnica Superior, University of Zaragoza, Crta. de Cuarte s/n, 22071 Huesca, Spain
* Correspondence: jmarinsaez@unizar.es

Abstract

Infrared optical vortices are used in the field of optical communications at wavelengths around 1550 nm. A versatile method to generate them is with a Spatial Light Modulator (SLM); however, they are expensive devices and cannot be easily integrated into compact systems, as opposed to Holographic Optical Elements (HOEs), which are lightweight, smaller and thinner, and easier to align and combine with other optical systems. In this work, volume transmission HOEs have been recorded in a commercial photopolymer, Bayfol HX200, by exposing it to the interference pattern obtained with an optical vortex (obtained with an SLM) and a plane wave in the visible range. When illuminated with a plane wave at 1534 nm, the diffracted beam carried an optical vortex. An experimental efficiency of approximately 45% at that wavelength has been obtained, proving the viability of the method.

Keywords: holographic optical elements; optical vortex; photopolymer; spatial light modulator

Received: 1 August 2025
Revised: 12 September 2025
Accepted: 19 September 2025
Published: 20 September 2025

Citation: Paredes-Amorín, Á.; Marín-Sáez, J.; Collados, M.-V.; Atencia, J. Infrared Optical Vortices Generation with Holographic Optical Elements Recorded in Bayfol HX200 Photopolymer. *Photonics* **2025**, *12*, 940. https://doi.org/10.3390/photonics12090940

1. Introduction

An optical vortex beam has a phase singularity at its center, where the intensity is zero, and the phase changes helicoidally around it:

$$\Phi = m\theta, \tag{1}$$

where m is the topological charge, that is, the number of 2π-phase jumps around the singularity per wavelength. This type of beam carries orbital angular momentum (OAM) [1].

Optical vortices can be obtained with several methods. For example, spiral phase plates introduce an additional optical path with an azimuth angle so that the phase changes helicoidally [2]; cylindrical lenses may be used to convert Hermite–Gaussian modes into Laguerre–Gaussian modes [3]; Q-plates allow the transfer of angular momentum from spin to orbital [4]; computer-generated holograms (CGHs) make use of the interference pattern of an optical vortex and a reference beam, a grating with a dislocation in the case of plane waves, so that when they are illuminated with the reference beam, the diffracted wave contains an optical vortex. This pattern may be written in a photographic film [5] or generated in a liquid crystal device, such as a Spatial Light Modulator (SLM) [6]. The latter is a versatile tool, since the CGH can be modified dynamically in order to obtain an optical vortex with a different topological charge, or for a different wavelength of illumination.

Optical vortices are used in a wide range of fields: microscopy [7], metrology [8], optical tweezers [9], condensed matter physics [10], quantum communications [11], nonlinear optics [12], and optical communications [13–15], to name a few. For this last application, the illumination wavelength must be in the infrared range, around 1550 nm.

Although there are SLMs suitable for infrared, they are expensive devices, have a low damage threshold, and their alignment and combination with other optical systems into a compact device is not simple.

A solution is to generate an optical vortex in the visible spectrum with an SLM and record its interference with another wave on a holographic material, such as a photopolymer or dichromated gelatin emulsion. The recording needs to be carried out in the visible spectrum because there are no holographic recording materials that are sensitive to infrared. The resulting HOE can then be illuminated with infrared light to obtain an optical vortex in that spectral range. HOEs are lightweight, smaller, and thinner, and it is easier to integrate them into compact systems, such as uniaxial elements or a combination of HOEs to achromatize a vortex beam [16]. Although this method has been used in the near infrared regime (around 800 nm) [16], to the authors' knowledge, it has not been used for wavelengths further away from the visible spectrum, such as the ones needed for optical communications, around 1550 nm.

The aim of this paper is to obtain an HOE that generates an optical vortex when illuminated at 1550 nm. The optical vortex needed for the holographic recording is, in turn, produced with an SLM due to its versatility.

2. Materials and Methods

2.1. Generation of Optical Vortices with a Spatial Light Modulator (SLM)

The PLUTO VIS *Phase Only* Spatial Light Modulator (*HoloEye*) was used to generate an optical vortex. It is an LCoS device, with 1080 × 1920 pixels, of 8 µm size.

The phase of the interference pattern of two plane waves, one of which was carrying an optical vortex, was calculated and displayed on the SLM. Figure 1 shows the pattern where the topological charge of the vortex is $m = 1$ (left) and $m = 2$ (right).

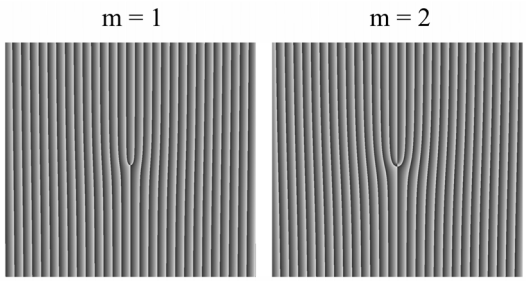

Figure 1. Interference pattern of a plane wave and a vortex with topological charge $m = 1$ (**left**) and $m = 2$ (**right**).

2.2. Design and Recording of Holographic Optical Elements

As mentioned before, there are no holographic recording materials sensitive to infrared, so HOEs have to be recorded with visible light. The commercial photopolymer Bayfol HX200 [17], sensitive to the whole visible spectrum and with a thickness of 16 µm, was chosen for this study. It presents good light sensitivity, low shrinkage, and no chemical or thermal post-processing needed, only photocuring with incoherent light.

Volume transmission HOEs were recorded at 532 nm with a Coherent Verdi V6 CW laser and the setup shown in Figure 2, with a recorded area diameter of approximately 1 cm. The laser beam was split into two, which interfered at the photosensitive material plane, with an angle between beams of 32°. One of the beams, the object beam, illuminated

the SLM described in the previous subsection, so that it carried OAM. A 4f processor was used in the object beam in order to cancel phase propagation terms and filter the optical vortex [18].

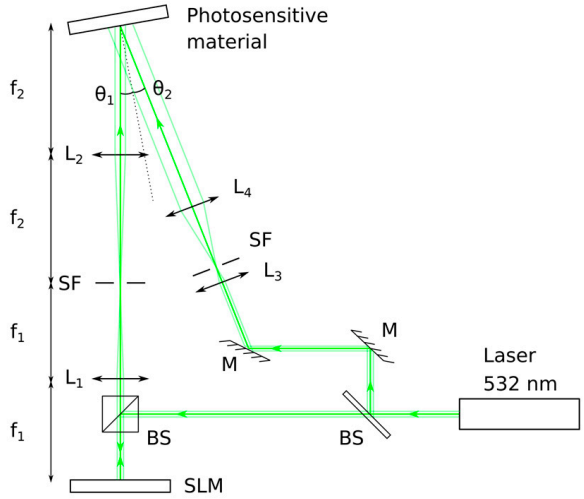

Figure 2. Holographic recording setup. M: mirror; BS: beam splitter; L: lens; SF: spatial filter; SLM: spatial light modulator; θ_1 and θ_2: recording angles in air; f_x: focal length of lens x (f_1 = 150 mm, f_2 = 150 mm, f_4 = 200 mm, and L_3 is a × 10 microscope objective).

The spatial period of the resulting interference pattern Λ at the photosensitive material plane (sufficiently far away from the dislocation) is given by Bragg's equation [19]:

$$\Lambda = \frac{\lambda}{2n \sin \theta'}, \tag{2}$$

where λ is the wavelength inside the recording medium, which has refractive index n, and θ' is the half-angle between the recording beams inside the medium. The spatial period needs to be large enough so that no total internal reflection occurs when reconstructing at wavelengths around 1550 nm.

The exposure dosage to record the HOEs was 16 mJ/cm^2, since in previous works, it was determined that it was necessary to obtain maximal refractive index modulation within the selected recording material for this spatial period, approximately n_1 = 0.024 [20]. This value is a limitation of the recording material itself.

The recording parameters are summarized in Table 1. They ensure that the resulting HOEs operate in the volume regime when reconstructing with wavelengths around 532 nm and longer.

Table 1. Recording parameters of the HOEs recorded with the setup shown in Figure 2.

Recording Wavelength (nm)	$\theta_{1,\,air}$ (°)	$\theta_{2,\,air}$ (°)	Λ (μm)	Exposure Dosage (mJ/cm^2)
532	16.0	−16.0	0.965	16.0

After the recording, the resulting holograms were bleached using the post-processing described in a previous work [21]: illumination with a 50 W white LED for 25 min.

2.3. Characterization of Holographic Optical Elements

When a volume HOE is reconstructed, or illuminated, the energy of the incident beam is distributed between the diffracted beam (+1 order) and the transmitted beam (0 order), depending on the illumination wavelength and angle. The efficiency of the HOE is maximal,

that is, as much energy as possible is in the diffracted beam, when the Bragg condition (Equation (2)) is fulfilled. That means that for each wavelength, there is an incidence angle θ_0, called the Bragg angle, that provides maximal efficiency. In that case, the efficiency is the following, according to Kogelnik's theory for volume HOEs [22]:

$$\eta = \sin^2\left(\frac{\pi n_1 d}{\lambda\sqrt{\cos\theta'_0\cos\theta'_{+1}}}\right) = \sin^2\left(\frac{\pi n_1 d}{\lambda\cos\theta'_0}\right), \tag{3}$$

where n_1 is the refractive index modulation achieved during the recording, d is the thickness of the recording material, λ is the reconstruction wavelength, and θ'_0 and θ'_{+1} are the angles of the propagation vectors of the transmitted and diffracted beam, respectively, inside the medium. The angle of the diffracted beam θ'_{+1} is obtained with Equation (2), and since the HOEs are recorded with unslanted geometry (both recording angles are the same in absolute value), the illumination angle that fulfills the Bragg condition at the reconstruction (θ'_0) is the same as the diffracted beam angle (θ'_{+1}) in absolute value. The efficiency of an HOE can be 100% if the Bragg condition is met and n_1 is the appropriate one for the wavelength and angles that fulfill the condition.

The efficiency was obtained experimentally by measuring the intensity of the diffracted beam I_{+1} and that of the transmitted beam, I_0, at the Bragg angle for each wavelength:

$$\eta = \frac{I_{+1}}{I_0 + I_{+1}} \tag{4}$$

Measurements were carried out for two wavelengths: at 532 nm with the laser used for the recording step and at 1534 nm with a tunable laser 8164B Lightwave Measurement system (Agilent Technologies, Santa Clara, CA USA) with a spectral width of less than 1 nm. In both cases, the beam diameter was approximately 2 mm.

In order to characterize the optical vortex present in the diffracted beam, two kinds of measurements were carried out. Firstly, the intensity profile of the beam was obtained with a CCD sensor camera. GigE (TheImagingSource, Bremen, Germany) CCD was used for the measurements at 532 nm, with dimensions of 1280 × 960 pixels and a pixel size of 3.75 µm, and Bobcat-320 (Xenics, Exosens Group, Leuven, Belgium) for measurements at 1534 nm, with 320 × 256 pixels and a pixel size of 20 µm. Secondly, in order to evaluate the phase of the aforementioned beam, an interferometer setup was prepared (as shown in Figure 3 for 1534 nm, and a similar setup for 532 nm), and the interference of the optical vortex produced by the HOE and a plane wave was visualized with the corresponding CCD camera.

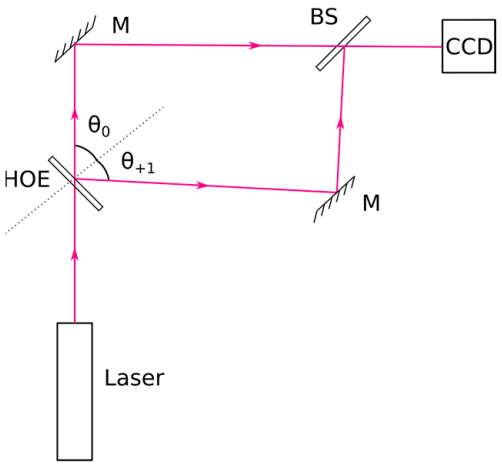

Figure 3. Interferometry setup for 1534 nm.

3. Results and Discussion

3.1. Optical Vortex Generation with a Spatial Light Modulator

Optical vortices with topological charge $m = 1$ and $m = 2$ were obtained with the SLM as explained in Section 2.1 at 532 nm. Figure 4 shows the intensity profile of the vortices when propagated to the photosensitive material plane in Figure 2, measured with the CCD camera mentioned in Section 2.3. The vortex characteristic ring shape is observed, as expected, as well as the width of the central area with no intensity, bigger in the case of higher topological charge. These optical vortices were used as object beams in the holographic recording setup of Figure 2.

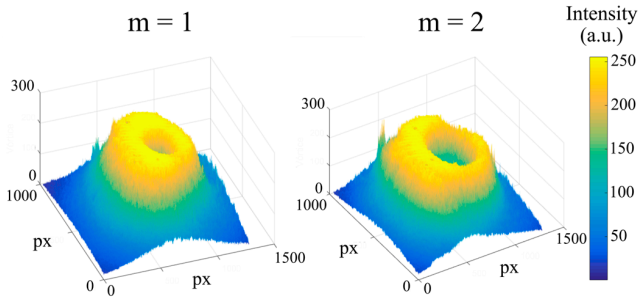

Figure 4. Intensity profile of the optical vortex generated at 532 nm with the SLM with topological charge m = 1 (**left**) and m = 2 (**right**). The horizontal axes represent pixels, and the vertical axis represents the intensity in arbitrary units.

3.2. Characterization of the Resulting Holographic Optical Element

Two HOEs were recorded at 532 nm with the setup explained in Section 2.2, each with an optical vortex with topological charge $m = 1$ or $m = 2$, respectively, shown in Section 3.1. Their theoretical efficiencies when reconstructed at 532 and 1534 nm with Bragg incidence were calculated using Kogelnik's Coupled Wave theory [22] with $n_1 = 0.024$, as explained in Section 2.2, and are shown in Table 2. The value of n_1 needed to obtain 100% efficiency at 532 nm is 0.016, lower than the value achieved during the recording. Thus, the HOEs are overmodulated for this wavelength, and the efficiency is lower than 100%, as can be derived from Equation (3). On the other hand, for 100% efficiency at 1534 nm, higher index modulation would be needed: 0.041, which cannot be obtained with Bayfol HX200 for the spatial period of the HOE, as determined in previous work [20].

Table 2. Bragg angle for the considered reconstruction wavelengths of the recorded HOE and theoretical and experimental efficiency.

Reconstruction Wavelength (nm)	$\theta_{0,\,Bragg,\,air}$ (°)	Theoretical Efficiency (%)	Experimental Efficiency (%)
532	16.0	55	55
1534	52.6	64	45

The efficiencies of both elements were also measured with the same conditions (Bragg incidence for each of the two wavelengths), as described in Section 2.3, and the results are included in Table 2 as well. As expected, the experimental result at 532 nm matches the theoretical one. However, the experimental efficiency for 1534 nm is significantly lower than the calculated one. The index modulation has been previously characterized [20], and it was validated with the measurement at 532 nm, so it would appear that it is not the cause of this difference. One possible explanation is that the refractive index of materials is lower for longer wavelengths [23], so it might be the case that the index modulation at 1534 nm is

lower than that in the visible range. In any case, a recording material that could provide $n_1 = 0.041$ would be desirable in the interest of achieving 100% efficiency at 1534 nm.

In order to characterize the optical vortex obtained in the diffracted beam for each of the two HOEs, its intensity profile was visualized with a CCD camera, as explained in Section 2.3. Figures 5 and 6 show this for 532 and 1534 nm, respectively, where the ring-shaped intensity distribution is clearly seen. As illustrated in Figure 2, the central dark area is larger in the case of higher topological charge. The interference pattern that is visible in the figures is believed to be caused by the interference of multiple reflections in the filter of the CCD camera.

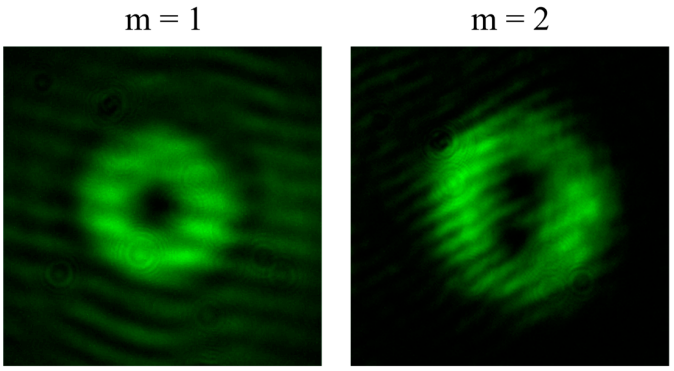

Figure 5. Intensity profile of the optical vortex with topological charge $m = 1$ (**left**) and $m = 2$ (**right**) obtained with the corresponding HOE at λ = 532 nm.

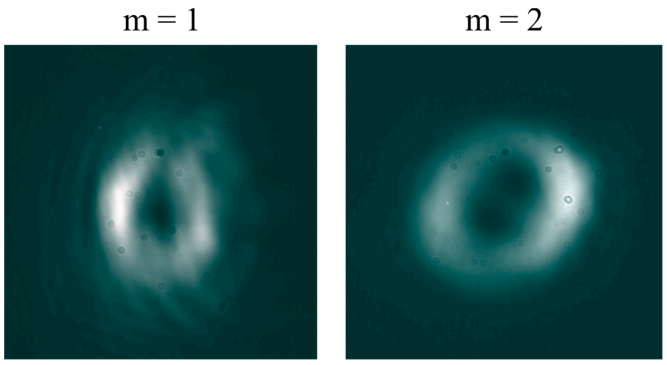

Figure 6. Intensity profile of the optical vortex with topological charge $m = 1$ (**left**) and $m = 2$ (**right**) obtained with the corresponding HOE at λ = 1534 nm.

Lastly, the interference of the optical vortex generated in the diffracted beam and a plane wave, as explained in Figure 3, is presented in Figures 7 and 8 for 532 and 1534 nm, respectively. As expected, in the case of $m = 1$, one fringe is divided into two in the dislocation, whereas for $m = 2$, one fringe is divided into three.

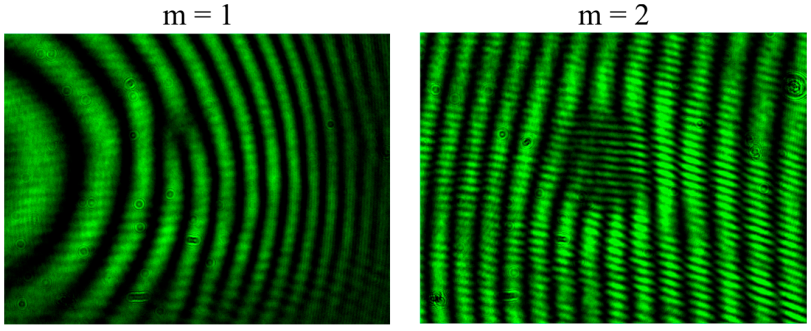

Figure 7. Interference pattern of a plane wave and the optical vortex with topological charge $m = 1$ (**left**) and $m = 2$ (**right**) obtained with the corresponding HOE at λ = 532 nm.

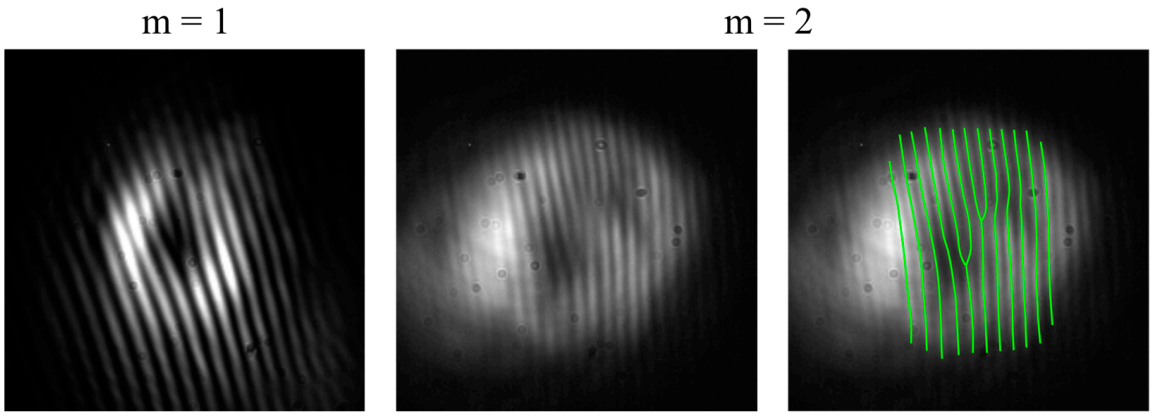

Figure 8. Interference pattern of a plane wave and the optical vortex with topological charge $m = 1$ (**left**) and $m = 2$ (**center** and **right**) obtained with the corresponding HOE at λ = 1534 nm.

4. Conclusions

Two volume transmission HOEs have been recorded at 532 nm with a plane wave and an optical vortex (with topological charges $m = 1$ and 2, respectively, generated by an SLM). When illuminating the HOE at 1534 nm, an optical vortex is obtained in the diffracted beam. The experimental efficiency at 532 nm matches the theoretical one, but at 1534 nm, it is approximately 45%, which is lower than the theoretical one (64%). Therefore, further analysis of the refractive index behavior for this wavelength should be carried out, as well as the use of a recording material that provides higher index modulation in order to obtain 100% efficiency. Nevertheless, the working principle has been proven, and it could be useful for applications in the communications field, among others.

Author Contributions: Conceptualization, J.A. and M.-V.C.; methodology, J.A. and M.-V.C.; investigation, Á.P.-A. and J.M.-S.; writing—original draft preparation, J.M.-S.; writing—review and editing, J.M.-S., J.A. and M.-V.C.; project administration, J.A. and M.-V.C.; funding acquisition, J.A. and M.-V.C. All authors have read and agreed to the published version of the manuscript.

Funding: This research was funded by the Spanish Ministerio de Ciencia, Innovación y Universidades and Agencia Estatal de Investigación (PID2024-157166NB-I00 and PID2020-114311RA-I00), Departamento de Industria e Innovación del Gobierno de Aragón (Grupo TOL, E44-23R) and University of Zaragoza (JIUZ2024-CIE-08).

Informed Consent Statement: Not applicable.

Data Availability Statement: Data is contained within the article.

Conflicts of Interest: The authors declare no conflicts of interest.

References

1. Allen, L.; Beijersbergen, M.W.; Spreeuw, R.J.C.; Woerdman, J.P. Orbital angular momentum of light and the transformation of Laguerre-Gaussian laser modes. *Phys. Rev. A* **1992**, *45*, 8185–8189. [CrossRef] [PubMed]
2. Beijersbergen, M.W.; Coerwinkel, R.P.C.; Kristensen, M.; Woerdman, J.P. Helical-wavefront laser beams produced with a spiral phaseplate. *Opt. Commun.* **1994**, *112*, 321–327. [CrossRef]
3. Beijersbergen, M.W.; Allen, L.; van der Veen, H.E.L.O.; Woerdman, J.P. Astigmatic laser mode converters and transfer of orbital angular momentum. *Opt. Commun.* **1993**, *96*, 123–132. [CrossRef]
4. Marrucci, L.; Manzo, C.; Paparo, D. Optical Spin-to-Orbital Angular Momentum Conversion in Inhomogeneous Anisotropic Media. *Phys. Rev. Lett.* **2006**, *96*, 163905. [CrossRef] [PubMed]
5. Bazhenov, V.Y.; Soskin, M.S.; Vasnetsov, M.V. Screw Dislocations in Light Wavefronts. *J. Mod. Opt.* **1992**, *39*, 985–990. [CrossRef]
6. Tao, S.H.; Lee, W.M.; Yuan, X.-C. Dynamic optical manipulation with a higher-order fractional Bessel beam generated from a spatial light modulator. *Opt. Lett.* **2003**, *28*, 1867–1869. [CrossRef] [PubMed]

7. Zou, H.; Zhong, S.; Lu, Y.; Zeng, K.; Ling, F.; Xu, L.; Liu, Y.; Chen, W.; Jiang, X. Vortex beam dynamic speckle interference microscopy. *Opt. Lett.* **2025**, *50*, 3676–3679. [CrossRef] [PubMed]
8. Cheng, M.; Jiang, W.; Guo, L.; Li, J.; Forbes, A. Metrology with a twist: Probing and sensing with vortex light. *Light Sci. Appl.* **2025**, *14*, 4. [CrossRef] [PubMed]
9. Yang, Y.; Ren, Y.-X.; Chen, M.; Arita, Y.; Rosales-Guzmán, C. Optical trapping with structured light: A review. *Adv. Photonics* **2021**, *3*, 034001. [CrossRef]
10. Rosen, G.F.Q.; Tamborenea, P.I.; Kuhn, T. Interplay between optical vortices and condensed matter. *Rev. Mod. Phys.* **2022**, *94*, 035003. [CrossRef]
11. Erhard, M.; Fickler, R.; Krenn, M.; Zeilinger, A. Twisted photons: New quantum perspectives in high dimensions. *Light Sci. Appl.* **2017**, *7*, 17146. [CrossRef] [PubMed]
12. Sola, I.J.; Collados, V.; Plaja, L.; Méndez, C.; Román, J.S.; Ruiz, C.; Arias, I.; Villamarín, A.; Atencia, J.; Quintanilla, M.; et al. High power vortex generation with volume phase holograms and non-linear experiments in gases. *Appl. Phys. B* **2008**, *91*, 115–118. [CrossRef]
13. Willner, A.E.; Pang, K.; Song, H.; Zou, K.; Zhou, H. Orbital angular momentum of light for communications. *Appl. Phys. Rev.* **2021**, *8*, 041312. [CrossRef]
14. Ma, M.; Lian, Y.; Wang, Y.; Lu, Z. Generation, Transmission and Application of Orbital Angular Momentum in Optical Fiber: A Review. *Front. Phys.* **2021**, *9*, 773505. [CrossRef]
15. Wang, J.; Chen, S.; Liu, J. Orbital angular momentum communications based on standard multi-mode fiber (invited paper). *APL Photonics* **2021**, *6*, 060804. [CrossRef]
16. Atencia, J.; Collados, M.-V.; Quintanilla, M.; Marín-Sáez, J.; Sola, Í.J. Holographic optical element to generate achromatic vórtices. *Opt. Express* **2013**, *21*, 21056–21061. [CrossRef] [PubMed]
17. Covestro Deutschland AG. Bayfol HX200 Datasheet. Available online: https://solutions.covestro.com/es/products/bayfol/bayfol-hx200_00000000086194384?SelectedCountry=ES (accessed on 18 September 2025).
18. Sacks, Z.S.; Rozas, D.; Swartzlander, G.A., Jr. Holographic formation of optical-vortex filaments. *J. Opt. Soc. Am. B* **1998**, *15*, 2226–2234. [CrossRef]
19. Syms, R. *Practical Volume Holography*; Oxford University Press: Oxford, UK, 1990.
20. Marín-Sáez, J.; Atencia, J.; Chemisana, D.; Collados, M.-V. Full modeling and experimental validation of cylindrical holographic lenses recorded in Bayfol HX photopolymer and partly operating in the transition regime for solar concentration. *Opt. Express* **2018**, *26*, A398–A412. [CrossRef] [PubMed]
21. Marín-Sáez, J.; Atencia, J.; Chemisana, D.; Collados, M.-V. Characterization of volume holographic optical elements recorded in Bayfol HX photopolymer for solar photovoltaic applications. *Opt. Express* **2016**, *24*, A720–A730. [CrossRef] [PubMed]
22. Kogelnik, H. Coupled wave theory for thick hologram gratings. *Bell Syst. Tech. J.* **1969**, *48*, 2909–2947. [CrossRef]
23. Hecht, E. *Optics*; Addison Wesley: Boston, MA, USA, 1998.